A Description of a Three-Dimensional Coastal Ocean Circulation Model

Alan F. Blumberg and George L. Mellor

Reprinted from:
Three Dimensional Coastal Ocean Models, by Norman S. Heaps (Editor), 1-16.

A DESCRIPTION OF A THREE-DIMENSIONAL COASTAL OCEAN CIRCULATION MODEL

Alan F. Blumberg[1]

Dynalysis of Princeton, Princeton, New Jersey 08540

George L. Mellor

Geophysical Fluid Dynamics Program, Princeton University, Princeton, New Jersey 08544

Abstract. A three-dimensional, primitive equation, time-dependent, σ coordinate, free surface, estuarine and coastal ocean circulation model is described in detail. An apparently unique feature is its imbedded turbulent closure submodel which on the basis of previous studies should yield realistic, Ekman surface and bottom layers. The model has been designed to represent ocean physics as realistically as possible given the present-day state of the art and to address phenomena of 1-100 km length and tidal-monthly time scales depending on basin size and grid resolution. The prognostic variables are the three components of the velocity field, temperature, salinity, and two quantities which characterize the turbulence, the turbulence kinetic energy and the turbulence macroscale. The governing equations together with their boundary conditions are solved by finite difference techniques. A horizontally and vertically staggered lattice of grid points is used for the computations. An implicit numerical scheme in the vertical direction and a mode splitting technique in time have been adopted for computational efficiency. The numerics have been designed to readily accommodate the highly time-dependent and often nonlinear processes of coastal upwelling and eddy dynamics. The numerical model incorporates realistic coastline and bottom topography. The actual computer code is configured to take advantage of the array processing design of modern computers so that long-term integrations are possible at tolerable cost. Applications of the model to a variety of coastal settings all produce circulation predictions which seem quite realistic when compared to the available data/theory. These applications include a simulation of the tides in the Chesapeake Bay, a simulation of the coastal circulation off Long Island, New York, and a computation of the general circulation in the Middle and South Atlantic Bights and in the Gulf of Mexico. The grid spacings have ranged from 1 to 50 km in these applications. In a new application to coastal upwelling, the model's behavior is in accord with recently developed ideas of coastal trapped waves.

1. Introduction

The coastal ocean is a region receiving a great deal of attention due to an increasing utilization of its resources. The demands for increasing development have directed both governments and individuals to investigate the basic mechanisms which govern the circulation over the continental shelf. A knowledge of the circulation is useful to the management of fisheries and of oil and gas resource development. Spills of oil and other material from offshore drilling and oil transport activities may occur and significantly affect the environment. Therefore, the movement of these pollutants becomes an important item to predict.

The purpose of this paper is to provide a relatively detailed description of a numerical circulation model developed over the last few years at Princeton University and Dynalysis of Princeton. The model belongs to that class of models where model realism is an important goal and addresses mesoscale phenomena, that is activity characterized by 1-100 km length and tidal-30 day time scales commonly observed in estuaries and the coastal ocean [Beardsley and Boicourt, 1981]. It is envisioned that the model ultimately will be used as part of a coastal ocean forecasting program. The model is a three-dimensional coastal ocean model, incorporating a turbulence closure model to provide a realistic parameterization of the vertical mixing processes. The prognostic variables are the three components of velocity, temperature, salinity, turbulence kinetic energy, and turbulence macroscale. The momentum equations are nonlinear and incorporate a variable Coriolis parameter. Prognostic equations governing the thermodynamic quantities, temperature, and salinity account for water mass variations brought about by highly time-dependent coastal upwelling

[1]Now at HydroQual, Inc., Mahwah, NJ 07430.

processes as well as horizontal advective processes. Free surface elevation is also calculated prognostically, with only some sacrifice in computational time so that tides and storm surge events can also be simulated. This is accomplished by use of a mode splitting technique whereby the volume transport and vertical velocity shear are solved separately. Other computer variables include the density, vertical eddy viscosity, and vertical eddy diffusivity. The model also accommodates realistic coastline geometry and bottom topography.

The model performance has been tested in a variety of applications which will not be described. To gain some appreciation for the model's ability to simulate coastal circulation the reader is referred to Blumberg [1977], and Blumberg and Mellor [1979a, b, 1980, 1981a, b, 1983]. These applications include a simulation of the tides in the Chesapeake Bay, a simulation of the coastal circulation off Long Island, New York, and a computation of the general circulation in the Middle Atlantic and South Atlantic Bights and in the Gulf of Mexico. The grid spacings have ranged from 1 to 50 km in these applications. Additional numerical experiments involving upwelling and coastal trapped waves will be described in this paper to provide an illustration of the utility of the model.

2. The Governing Equations

Dynamic and Thermodynamic Equations

The equations which form the basis of the circulation model describe the velocity and surface elevation fields, and the salinity and temperature fields. Two simplifying approximations are used [Bryan, 1969]; first, it is assumed that the weight of the fluid identically balances the pressure (hydrostatic assumption), and second, density differences are neglected unless the differences are multiplied by gravity (Boussinesq approximation).

Consider a system of orthogonal Cartesian coordinates with x increasing eastward, y increasing northward, and z increasing vertically upwards. The free surface is located at $z = \eta(x,y,t)$ and the bottom is at $z = -H(x,y)$. If $\underset{\rightarrow}{V}$ is the horizontal velocity vector with components (U,V) and ∇ the horizontal gradient operator, the continuity equation is

$$\nabla \cdot \underset{\rightarrow}{V} + \frac{\partial W}{\partial z} = 0 \tag{1}$$

The Reynolds momentum equations are

$$\frac{\partial U}{\partial t} + \underset{\rightarrow}{V} \cdot \nabla U + W \frac{\partial U}{\partial z} - fV = -\frac{1}{\rho_o}\frac{\partial P}{\partial x} + \frac{\partial}{\partial z}\left(K_M \frac{\partial U}{\partial z}\right) + F_x \tag{2}$$

$$\frac{\partial V}{\partial t} + \underset{\rightarrow}{V} \cdot \nabla V + W \frac{\partial V}{\partial z} + fU = -\frac{1}{\rho_o}\frac{\partial P}{\partial y} + \frac{\partial}{\partial z}\left(K_M \frac{\partial V}{\partial z}\right) + F_y \tag{3}$$

$$\rho g = -\frac{\partial P}{\partial z} \tag{4}$$

with ρ_o the reference density, ρ the in situ density, g the gravitational acceleration, P the pressure, K_M the vertical eddy diffusivity of turbulent momentum mixing. A latitudinal variation of the Coriolis parameter, f, is introduced by use of the β plane approximation.

The pressure at depth z can be obtained by integrating the vertical component of the equation of motion, (4), from z to the free surface η, and is

$$P(x,y,z,t) = P_{atm} + g\rho_o\eta + g\int_z^0 \rho(x,y,z',t)dz' \tag{5}$$

Henceforth, the atmospheric pressure, P_{atm} is assumed constant.

The conservation equations for temperature and salinity may be written as

$$\frac{\partial \Theta}{\partial t} + \underset{\rightarrow}{V} \cdot \Delta\Theta + W\frac{\partial \Theta}{\partial z} = \frac{\partial}{\partial z}\left(K_H \frac{\partial \Theta}{\partial z}\right) + F_\Theta \tag{6}$$

$$\frac{\partial S}{\partial t} + \underset{\rightarrow}{V} \cdot \nabla S + W \frac{\partial S}{\partial z} = \frac{\partial}{\partial z}\left(K_H \frac{\partial S}{\partial z}\right) + F_S \tag{7}$$

where Θ is the potential temperature (or in situ temperature for shallow water applications) and S is the salinity. The vertical eddy diffusivity for turbulent mixing of heat and salt is denoted as K_H. Using the temperature and salinity, the density is computed according to an equation of state of the form

$$\rho = \rho(\Theta,S) \tag{8}$$

given by Fofonoff [1962]. The potential density is ρ, that is, the density evaluated as a function of potential temperature and salinity but at atmospheric pressure; it provides accurate density information to calculate horizontal baroclinic gradients which enter in the pressure gradient terms and the vertical stability of the water column which enters into the turbulence closure model even in deep water when pressure effects become important.

All of the motions induced by small-scale processes not directly resolved by the model grid (subgrid scale) is parameterized in terms of horizontal mixing processes. The terms F_x, F_y, F_Θ and

F_S found in (2), (3), (6), and (7) represent these unresolved processes and in analogy to molecular diffusion can be written as

$$F_x = \frac{\partial}{\partial x}\left[2A_M \frac{\partial U}{\partial x}\right] + \frac{\partial}{\partial y}\left[A_M\left(\frac{\partial U}{\partial y} + \frac{\partial V}{\partial x}\right)\right] \quad (9a)$$

$$F_y = \frac{\partial}{\partial y}\left[2A_M \frac{\partial V}{\partial y}\right] + \frac{\partial}{\partial x}\left[A_M\left(\frac{\partial U}{\partial y} + \frac{\partial V}{\partial x}\right)\right] \quad (9b)$$

and

$$F_{\Theta,S} = \frac{\partial}{\partial x} A_H \frac{\partial(\Theta,S)}{\partial x} + \frac{\partial}{\partial y} A_H \frac{\partial(\Theta,S)}{\partial y} \quad (10)$$

One should note that F_x and F_y are invariant to coordinate rotation. While, these horizontal diffusive terms are meant to parameterize subgrid scale processes, in practice the horizontal diffusivities, A_M and A_H, are usually required to damp small-scale computational noise. The form of F_x, F_y and $F_{\Theta,S}$ allows for variable A_M and A_H but thus far they have been held constant. The diffusivities are chosen so that they do not produce excessive smoothing of real features. Values as low as 10 m^2/s have been used successfully in various applications. The relatively fine vertical resolution used in the applications resulted in a reduced need for horizontal diffusion because horizontal advection followed by vertical mixing effectively acts like horizontal diffusion in a real physical sense. An enhancement, now in progress, is to relate A_M and A_H to the scales of motion being resolved in the model and to the local deformation field as suggested by Smagorinsky [1963].

Turbulence Closure

The governing equations contain parameterized Reynolds stress and flux terms which account for the turbulent diffusion of momentum, heat, and salt. The parameterization of turbulence in the model described here is based on the work of Mellor and Yamada [1974].

The vertical mixing coefficients, K_M and K_H, in (2), (3), (6), and (7) are obtained by appealing to a second order turbulence closure scheme [Mellor and Yamada, 1982] which characterizes the turbulence by equations for the turbulence kinetic energy, $q^2/2$, and a turbulence macroscale, ℓ, according to,

$$\frac{\partial q^2}{\partial t} + \underset{\sim}{V}\cdot\nabla q^2 + W\frac{\partial q^2}{\partial z} = \frac{\partial}{\partial z}\left(K_q \frac{\partial q^2}{\partial z}\right) + 2K_M\left[\left(\frac{\partial U}{\partial z}\right)^2 + \left(\frac{\partial V}{\partial z}\right)^2\right] + \frac{2g}{\rho_o} K_H \frac{\partial \rho}{\partial z} - \frac{2q^3}{B_1 \ell} + F_q \quad (11)$$

and

$$\frac{\partial q^2 \ell}{\partial t} + \underset{\sim}{V}\cdot\nabla(q^2\ell) + W\frac{2q^2\ell}{\partial z} = \frac{\partial}{\partial z}\left[K_q \frac{\partial}{\partial z}(q^2\ell)\right] + \ell E_1 K_M\left[\left(\frac{\partial U}{\partial z}\right)^2 + \left(\frac{\partial V}{\partial z}\right)^2\right] + \frac{\ell E_1 g}{\rho_o} K_H \frac{\partial \rho}{\partial z} - \frac{q^3}{B_1}\tilde{W} + F_\ell \quad (12)$$

where a wall proximity function is defined as

$$\tilde{W} \equiv 1 + E_2\left(\frac{\ell}{\kappa L}\right)^2 \quad (13)$$

and where

$$(L)^{-1} \equiv (\eta - z)^{-1} + (H + z)^{-1} \quad (14)$$

Near surfaces it may be shown that both ℓ/κ and L are equal to the distance from the surface ($\kappa = 0.4$ is the von Karman constant) so that $\tilde{W} = 1 + E_2$. Far from the surfaces where $\ell << L$, $\tilde{W} \simeq 1$. The length scale provided by (12) is a characteristic length of the turbulent motion at any point in space or time. An alternative to (12) is to use a transport equation for the dissipation rate [Hanjalic and Launder, 1972]. The former approach according to Mellor and Herring [1973] and Mellor and Yamada [1982] is more consistent since it uses an equation which describes large-scale turbulence to determine the turbulent macroscale. The terms F_q and F_ℓ in (11) and (12) are the horizontal mixing and are parameterized analogously to temperature and salinity by using (10).

While details of the closure model are rather involved, it is possible to reduce the prescription of the mixing coefficients K_M, K_H, and K_q to the following expressions,

$$K_M \equiv \ell q S_M \quad (15a)$$

$$K_H \equiv \ell q S_H \quad (15b)$$

$$K_q \equiv \ell q S_q \quad (15c)$$

The stability functions, S_M, S_H, and S_q are analytically derived, algebraic relations functionally dependent upon $\partial U/\partial z$, $\partial V/\partial z$, $g\rho_o^{-1}\partial\rho/\partial z$, q and ℓ. These relations derive from closure hypotheses described by Mellor [1973] and recently summarized by Mellor and Yamada [1982].

It is convenient to define

$$G_m \equiv \frac{\ell^2}{q^2}\left[\left(\frac{\partial U}{\partial z}\right)^2 + \left(\frac{\partial V}{\partial z}\right)^2\right]^{1/2} \tag{16a}$$

$$G_H \equiv \frac{\ell^2}{q^2}\frac{g}{\rho_o}\frac{\partial \rho}{\partial z} \tag{16b}$$

Then the stability functions become

$$S_M\left[6A_1A_2G_M\right] + S_H\left[1 - 2A_2B_2G_H - 12A_1A_2G_H\right] = A_2 \tag{17a}$$

$$S_M\left[1 + 6A_1^2G_M - 9A_1A_2G_H\right] - S_H\left[12A_1^2G_H + 9A_1A_2G_H\right] = A_1(1 - 3C_1) \tag{17b}$$

$$S_q = 0.20 \tag{17c}$$

which are readily solved for S_M and S_H as functions of G_M and G_H. By appealing to laboratory data [Mellor and Yamada, 1982] (see section 6 for further practical details), the empirical constants were assigned the values

$$(A_1, A_2, B_1, B_2, C_1) = (0.92,\ 0.74,\ 16.6,\ 10.1,\ 0.08) \tag{18}$$

and

$$(E_1, E_2) = (1.8,\ 1.33) \tag{19}$$

Boundary Conditions

The boundary conditions at the free surface, $z = \eta(x,y)$, are

$$\rho_o K_M\left(\frac{\partial U}{\partial z},\ \frac{\partial V}{\partial z}\right) = (\tau_{ox},\ \tau_{oy}) \tag{20a}$$

$$\rho_o K_H\left(\frac{\partial \Theta}{\partial z},\ \frac{\partial S}{\partial z}\right) = (\dot{H},\ \dot{S}) \tag{20b}$$

$$q^2 = B_1^{2/3} u_{\tau s}^2 \tag{20c}$$

$$q^2\ell = 0 \tag{20d}$$

$$W = U\frac{\partial \eta}{\partial x} + V\frac{\partial \eta}{\partial y} + \frac{\partial \eta}{\partial t} \tag{20e}$$

where (τ_{ox}, τ_{oy}) is the surface wind stress vector with the friction velocity, $u_{\tau s}$, the magnitude of the vector. It is doubtful that the mixing length goes to zero at a surface containing wind induced waves as suggested by (20d). The error is incurred in the near surface layers of thickness of order of the wave height. This is an area where further improvement is necessary. The quantity $B_1^{2/3}$ is an empirical constant (6.51) arising from the turbulence closure relations. The net ocean heat flux is $\dot{H}$ and here $\dot{S} \equiv S(0)\,[\dot{E}-\dot{P}]/\rho_o$ where $(\dot{E}-\dot{P})$ is the net evaporation-precipitation fresh water surface mass flux rate and $S(0)$ is the surface salinity. On the side walls and bottom of the basin, the normal gradients of Θ and S are zero so that there are no advective and diffusive heat and salt fluxes across these boundaries. At the lower boundary (b),

$$\rho_o K_M\left(\frac{\partial U}{\partial z},\ \frac{\partial V}{\partial z}\right) = (\tau_{bx},\ \tau_{by}) \tag{21a}$$

$$q^2 = B_1^{2/3} u_{\tau b}^2 \tag{21b}$$

$$q^2\ell = 0 \tag{21c}$$

$$W_b = -U_b\frac{\partial H}{\partial x} - V_b\frac{\partial H}{\partial y} \tag{21d}$$

where $H(x,y)$ is the bottom topography and $u_{\tau b}$ is the friction velocity associated with the bottom frictional stress (τ_{bx},τ_{by}). The bottom stress is determined by matching velocities with the logarithmic law of the wall. Specifically,

$$\vec{\tau}_b = \rho_o C_D |\vec{V}_b| \vec{V}_b \tag{22}$$

with value of the drag coefficient C_D given by

$$C_D = \left[\frac{1}{\kappa}\ln(H + z_b)/z_o\right]^{-2} \tag{23a}$$

where z_b and $\vec{V}_b$ are the grid point and corresponding velocity in the grid point nearest the bottom and κ is the von Karman constant. The final result of (22) and (23) in conjunction with the turbulent closure derived K_M is that the calculations will yield

$$\vec{V} = (\vec{\tau}_b/\kappa u_{\tau b})\ln(z/z_o) \tag{23b}$$

in the lower boundary region if enough resolution is provided. In those instances where the bottom boundary layer is not well resolved it is more appropriate to specify $C_D = 0.0025$. The actual algorithm is to set C_D to the larger of the two values given by (23a) and 0.0025. The parameter z_o depends on the local bottom roughness; in the absence of specific information $z_o = 1$ cm is used as suggested by Weatherly and Martin [1978].

Open lateral boundary conditions are problematic since one must parameterize the environment

exterior to the relevant domain. Two types of open boundaries exist, inflow and outflow. Temperature and salinity are prescribed from data at an inflowing boundary, whereas at outflow boundaries,

$$\frac{\partial}{\partial t}(\theta,S) + U_n \frac{\partial}{\partial n}(\theta,S) = 0 \qquad (23c)$$

is solved where the subscript n is the coordinate normal to the boundary. Turbulence kinetic energy and the macroscale quantity ($q^2\ell$) are calculated with sufficient accuracy at the boundaries by neglecting the advection in comparison with other terms in their respective equations.

The open lateral velocity boundary conditions in some of the applications are computed by using the available hydrographic data in conjunction with a simplified diagnostic model. This type of model uses only geostrophic plus Ekman dynamics and therefore solves a simplified form of the full equations of motion. It does not require a velocity at a reference level but only along a single transect crossing f/H contours. A detailed description of this model can be found in the work by Kantha et al. [1982]. While the normal component of velocity is specified, a free slip condition is used for the tangential component.

In other applications including those with tidal forcing, either the elevation is prescribed as a function of time and space or a radiation condition of the form

$$\frac{\partial \eta}{\partial t} + c \frac{\partial \eta}{\partial n} = F(s,t) \qquad (24)$$

is prescribed. Here c is the local shallow water wave speed, $(gH)^{1/2}$, and s is the tangential coordinate. The function F(s,t) incorporates the necessary forcing due to tides and the mean calculation as described by Blumberg and Kantha [1985]. The nonlinear terms in the momentum equations are additionally neglected at the open boundary.

Diagnostic Mode

Numerical experiments have been performed [Blumberg and Mellor, 1983] which involve the use of the circulation model in both prognostic and diagnostic modes. In the prognostic mode the momentum equations as well as equations governing the temperature and salinity distributions are integrated as an initial value problem. These predictive experiments do not always reach steady state since the oceanic response time for the density field can be considerable. As an alternative, diagnostic computations are considered.

In the diagnostic mode the observed density distribution is specified at all points in the grid and held fixed in time. The velocity field consistent with this constraint is allowed to spin up from rest. These experiments typically attain steady conditions after 10 days for even fairly large oceanic regions. The diagnostic approach not only provides a powerful tool for deducing the circulation but it also provides a consistent way of initializing a prognostic forecast model.

3. Vertical Coordinate Representation

It has often been noted that the ordinary x,y,z coordinate system has certain disadvantages in the vicinity of large bathymetric irregularities. It is desirable to introduce a new set of independent variables that transforms both the surface and the bottom into coordinate surfaces [Phillips, 1957]. The governing external and internal mode equations are transformed from (x,y,z,t) to (x*,y*,σ,t*) coordinates, where

$$x^* = x \qquad y^* = y \qquad \sigma = \frac{z-\eta}{H+\eta} \qquad t^* = t \qquad (25)$$

Now let $D \equiv H + \eta$ and apply the chain rule; the following relationships linking derivatives in the old system to those in the new system are obtained:

$$\frac{\partial G}{\partial x} = \frac{\partial G}{\partial x^*} - \frac{\partial G}{\partial \sigma}\left(\frac{\sigma}{D}\frac{\partial D}{\partial x^*} + \frac{1}{D}\frac{\partial \eta}{\partial x^*}\right) \qquad (26a)$$

$$\frac{\partial G}{\partial y} = \frac{\partial G}{\partial y^*} - \frac{\partial G}{\partial \sigma}\left(\frac{\sigma}{D}\frac{\partial D}{\partial y^*} + \frac{1}{D}\frac{\partial \eta}{\partial y^*}\right) \qquad (26b)$$

$$\frac{\partial G}{\partial z} = \frac{1}{D}\frac{\partial G}{\partial \sigma} \qquad (26c)$$

$$\frac{\partial G}{\partial t} = \frac{\partial G}{\partial t^*} - \frac{\partial G}{\partial \sigma}\left(\frac{\sigma}{D}\frac{\partial D}{\partial t^*} + \frac{1}{D}\frac{\partial \eta}{\partial t^*}\right) \qquad (26d)$$

where G is an arbitrary field available, and σ ranges from σ = 0 at z = η to σ = -1 at z = -H. A new vertical velocity can now be defined

$$\omega \equiv W - U\sigma\left(\frac{\partial D}{\partial x^*} + \frac{\partial \eta}{\partial x^*}\right) - V\sigma\left(\frac{\partial D}{\partial y^*} + \frac{\partial \eta}{\partial y^*}\right) - \left(\sigma\frac{\partial D}{\partial t^*} + \frac{\partial \eta}{\partial t^*}\right) \qquad (27)$$

which transforms the boundary conditions, (20e) and (21d), into

$$\omega(x^*,y^*,0,t^*) = 0 \qquad (28a)$$

$$\omega(x^*,y^*,-1,t^*) = 0 \qquad (28b)$$

Also, any vertically integrated quantity, G, for example, now appears as

$$\bar{G} = \int_{-1}^{0} G\, d\sigma \qquad (29)$$

Equations (1), (2), (3), (6), (7), (11), and (12) may now be written as (all asterisks will be dropped for notational convenience)

$$\frac{\partial \eta}{\partial t} + \frac{\partial UD}{\partial x} + \frac{\partial VD}{\partial y} + \frac{\partial \omega}{\partial \sigma} = 0 \tag{30}$$

$$\frac{\partial UD}{\partial t} + \frac{\partial U^2 D}{\partial x} + \frac{\partial UVD}{\partial y} + \frac{\partial U\omega}{\partial \sigma} - fVD + gD\frac{\partial \eta}{\partial x}$$
$$= \frac{\partial}{\partial \sigma}\left[\frac{K_M}{D}\frac{\partial U}{\partial \sigma}\right] - \frac{gD^2}{\rho_o}\frac{\partial}{\partial x}\int_\sigma^o \rho\, d\sigma$$
$$+ \frac{gD}{\rho_o}\frac{\partial D}{\partial x}\int_\sigma^o \sigma\frac{\partial \rho}{\partial \sigma}\, d\sigma + DF_x \tag{31}$$

$$\frac{\partial VD}{\partial t} + \frac{\partial UVD}{\partial x} + \frac{\partial V^2 D}{\partial y} + \frac{\partial V\omega}{\partial \sigma} + fUD + gD\frac{\partial \eta}{\partial y}$$
$$= \frac{\partial}{\partial \sigma}\left[\frac{K_M}{D}\frac{\partial V}{\partial \sigma}\right] - \frac{gD^2}{\rho}\frac{\partial}{\partial y}\int_\sigma^o \rho\, d\sigma$$
$$+ \frac{gD}{\rho_o}\frac{\partial D}{\partial y}\int_\sigma^o \sigma\frac{\partial \rho}{\partial \sigma}\, d\sigma + DF_y \tag{32}$$

$$\frac{\partial \Theta D}{\partial t} + \frac{\partial \Theta UD}{\partial x} + \frac{\partial \Theta VD}{\partial y} + \frac{\partial \Theta \omega}{\partial \sigma} = \frac{\partial}{\partial \sigma}\left[\frac{K_H}{D}\frac{\partial \Theta}{\partial \sigma}\right] + DF_\Theta \tag{33}$$

$$\frac{\partial SD}{\partial t} + \frac{\partial SUD}{\partial x} + \frac{\partial SVD}{\partial y} + \frac{\partial S\omega}{\partial \sigma} = \frac{\partial}{\partial \sigma}\left[\frac{K_H}{D}\frac{\partial S}{\partial \sigma}\right] + DF_S \tag{34}$$

$$\frac{\partial q^2 D}{\partial t} + \frac{\partial Uq^2 D}{\partial x} + \frac{\partial Vq^2 D}{\partial y} + \frac{\partial \omega q^2}{\partial \sigma} = \frac{\partial}{\partial \sigma}\left(\frac{K_q}{D}\frac{\partial q^2}{\partial \sigma}\right)$$
$$+ \frac{2K_M}{D}\left[\left(\frac{\partial U}{\partial \sigma}\right)^2 + \left(\frac{\partial V}{\partial \sigma}\right)^2\right] + \frac{2g}{\rho_o}K_H\frac{\partial \rho}{\partial \sigma} - \frac{2Dq^3}{\Lambda_1} + DF_q \tag{35}$$

$$\frac{\partial q^2 \ell D}{\partial t} + \frac{\partial Uq^2 \ell D}{\partial x} + \frac{\partial Vq^2 \ell D}{\partial y} + \frac{\partial \omega q^2}{\partial \sigma} = \frac{\partial}{\partial \sigma}\left(\frac{K_q}{D}\frac{\partial q^2 \ell}{\partial \sigma}\right)$$
$$+ E_1 \ell\left\{\frac{K_M}{D}\left[\left(\frac{\partial U}{\partial \sigma}\right)^2 + \left(\frac{\partial V}{\partial \sigma}\right)^2\right] + \frac{qE_3}{\rho_o}K_H\frac{\partial \rho}{\partial \sigma}\right\}$$
$$- \frac{Dq^3}{B_1}\tilde{W} + DF_\ell \tag{36}$$

The horizontal viscosity and diffusion terms are defined according to:

$$DF_x \equiv \frac{\partial \hat{\tau}_{xx}}{\partial x} - \frac{\partial}{\partial \sigma}\left[\left(\frac{\sigma}{D}\frac{\partial D}{\partial x} + \frac{1}{D}\frac{\partial \eta}{\partial x}\right)\hat{\tau}_{xx}\right]$$
$$+ \frac{\partial}{\partial y}(\hat{\tau}_{yx}) - \frac{\partial}{\partial \sigma}\left[\left(\frac{\sigma}{D}\frac{\partial D}{\partial y} + \frac{1}{D}\frac{\partial \eta}{\partial y}\right)\hat{\tau}_{yx}\right] \tag{37}$$

$$DF_y \equiv \frac{\partial \hat{\tau}_{yy}}{\partial y} - \frac{\partial}{\partial \sigma}\left[\left(\frac{\sigma}{D}\frac{\partial D}{\partial y} + \frac{1}{D}\frac{\partial \eta}{\partial y}\right)\hat{\tau}_{yy}\right]$$
$$+ \frac{\partial}{\partial x}(\hat{\tau}_{xy}) - \frac{\partial}{\partial \sigma}\left[\left(\frac{\sigma}{D}\frac{\partial D}{\partial x} + \frac{1}{D}\frac{\partial \eta}{\partial x}\right)\hat{\tau}_{xy}\right] \tag{38}$$

with

$$\hat{\tau}_{xx} = 2A_M\left[\frac{\partial UD}{\partial x} - \frac{\partial}{\partial \sigma}\left(\sigma\frac{\partial D}{\partial x} + \frac{\partial \eta}{\partial x}\right)U\right] \tag{39}$$

$$\hat{\tau}_{xy} = \hat{\tau}_{yx} = A_M\left[\frac{\partial UD}{\partial y} - \frac{\partial}{\partial \sigma}\left(\sigma\frac{\partial D}{\partial y} + \frac{\partial \eta}{\partial y}\right)U\right.$$
$$\left. + \frac{\partial VD}{\partial x} - \frac{\partial}{\partial \sigma}\left(\sigma\frac{\partial D}{\partial x} + \frac{\partial \eta}{\partial x}\right)V\right] \tag{40}$$

$$\hat{\tau}_{yy} = 2A_M\left[\frac{\partial VD}{\partial y} - \frac{\partial}{\partial \sigma}\left(\sigma\frac{\partial D}{\partial y} + \frac{\partial \eta}{\partial y}\right)V\right] \tag{41}$$

Also,

$$DF_{\Theta_i} = \frac{\partial \hat{q}_x}{\partial x} - \frac{\partial}{\partial \sigma}\left[\left(\frac{\sigma}{D}\frac{\partial D}{\partial x} + \frac{1}{D}\frac{\partial \eta}{\partial x}\right)\hat{q}_x\right]$$
$$+ \frac{\partial \hat{q}_y}{\partial y} - \frac{\partial}{\partial \sigma}\left[\left(\frac{\sigma}{D}\frac{\partial D}{\partial y} + \frac{\partial \eta}{\partial y}\right)\hat{q}_y\right] \tag{42}$$

$$\hat{q}_x = A_H\left[\frac{\partial \Theta_i D}{\partial x} - \frac{\partial}{\partial \sigma}\left(\sigma\frac{\partial D}{\partial x} + \frac{\partial \eta}{\partial x}\right)\Theta_i\right] \tag{43}$$

$$\hat{q}_y = A_H\left[\frac{\partial \Theta_i D}{\partial y} - \frac{\partial}{\partial \sigma}\left(\sigma\frac{\partial D}{\partial y} + \frac{\partial \eta}{\partial y}\right)\Theta_i\right] \tag{44}$$

where Θ_i now represents Θ, S, q^2 and $q^2\ell$.

Since the time this paper was accepted for publication, Mellor and Blumberg [1985] have shown that the conventional model for horizontal diffusion is incorrect when bottom topographical slopes are large. A new formulation has been suggested which is simpler than equations (37)-(44) and makes it possible to model realistically bottom boundary layers over sharply sloping bottoms.

4. Mode Splitting Technique

The equations governing the dynamics of coastal circulation contain propagation of fast moving external gravity waves and slow moving internal gravity waves. It is desirable in terms of computer economy to separate out vertically integrated equations (external mode) from the vertical structure equations (internal mode). This technique, known as mode splitting [see Simons, 1974; Madala and Piacsek, 1977] permits the calculation of the free surface elevation with little sacrifice in computational time by solving the volume transport separately from the vertical velocity shear.

The volume transport, external mode equations

are obtained by integrating the internal mode equations over the depth, thereby eliminating all vertical structure. By integrating (30) from $\sigma = -1$ to $\sigma = 0$ and using the boundary conditions (28a,b) an equation for the surface elevation can be written as

$$\frac{\partial \eta}{\partial t} + \frac{\partial \bar{U}D}{\partial x} + \frac{\partial \bar{V}D}{\partial y} = 0 \qquad (45)$$

and the momentum equations become upon vertical integration

$$\frac{\partial \bar{U}D}{\partial t} + \frac{\partial \bar{U}^2 D}{\partial x} + \frac{\partial \overline{UV}D}{\partial y} - f\bar{V}D + gD\frac{\partial \eta}{\partial x} - D\bar{F}_x = -\overline{wu}(0)$$

$$+ \overline{wu}(-1) - \frac{\partial \overline{DU'^2}}{\partial x} - \frac{\partial \overline{DU'V'}}{\partial y} - \frac{gD^2}{\rho_o}\frac{\partial}{\partial x}\int_{-1}^{0}\int_{\sigma}^{0} \rho d\sigma' d\sigma$$

$$+ \frac{gD}{\rho_o}\frac{\partial D}{\partial x}\int_{-1}^{0}\int_{\sigma}^{0} \sigma' \frac{\partial \rho}{\partial \sigma}\, d\sigma' d\sigma \qquad (46)$$

$$\frac{\partial \bar{V}D}{\partial t} + \frac{\partial \overline{UV}D}{\partial x} + \frac{\partial \bar{V}^2 D}{\partial y} + f\bar{U}D + gD\frac{\partial \eta}{\partial y} - D\bar{F}_y = -\overline{wv}(0)$$

$$+ \overline{wv}(-1) - \frac{\partial D\overline{U'V'}}{\partial x} - \frac{\partial \overline{DV'^2}}{\partial y} - \frac{gD^2}{\rho_o}\frac{\partial}{\partial y}\int_{-1}^{0}\int_{\sigma}^{0} \rho d\sigma' d\sigma$$

$$+ \frac{gD}{\rho_o}\frac{\partial D}{\partial y}\int_{-1}^{0}\int_{\sigma}^{0} \sigma' \frac{\partial \rho}{\partial \sigma'}\, d\sigma' d\sigma \qquad (47)$$

where the pressure has been obtained from (5) and the vertically integrated velocities are defined as

$$(\bar{U},\bar{V}) \equiv \int_{-1}^{0} (U,V)\, d\sigma \qquad (48)$$

The wind stress components are $-\overline{wu}(0)$, and $-\overline{wv}(0)$, and the bottom stress components are $-\overline{wu}(-1)$ and $-\overline{wv}(-1)$. The terms in (46) and (47) involving U'^2, $U'V'$, and V'^2 represent vertical averages of the cross-products of the velocity departures from the vertically integrated (average) velocity and are often denoted as the dispersion terms. Thus

$$(\overline{U'^2}, \overline{V'^2}, \overline{U'V'}) = \int_{-1}^{0} (U'^2, V'^2, U'V')d\sigma \qquad (49)$$

where $(U',V') = (U-\bar{U}, V-\bar{V})$. The quantities $\bar{F}_x$ and $\bar{F}_y$ are vertical integrals of the horizontal momentum diffusion and are defined according to

$$D\bar{F}_x = \frac{\partial}{\partial x}\left(2A_M \frac{\partial \bar{U}D}{\partial x}\right) + \frac{\partial}{\partial y} A_M \left(\frac{\partial \bar{U}D}{\partial y} + \frac{\partial \bar{V}D}{\partial x}\right) \qquad (50)$$

$$D\bar{F}_y = \frac{\partial}{\partial y}\left(2A_M \frac{\partial \bar{V}D}{\partial y}\right) + \frac{\partial}{\partial x} A_M \left(\frac{\partial \bar{U}D}{\partial y} + \frac{\partial \bar{V}D}{\partial x}\right) \qquad (51)$$

The computational strategy is to solve equations for the external mode, the shallow water wave equations (45), (46), and (47), with a short time step to resolve tidal motions. The external mode solutions are obtained with the terms on the right-hand side of (46) and (47) held fixed in time and after a large number of time steps, of the order of 100, an internal mode calculation is carried out. The external mode provides $\partial\eta/\partial x$ and $\partial\eta/\partial y$ for insertion into the internal mode equations, (30) through (36), which are then solved with a much longer time step. Once the vertical structure has been determined, the terms on the right-hand side (46) and (47) are updated and another external mode solution begins. In future simulations, the advective and diffusive terms in (46) and (47) will be supplied by the internal mode.

The external mode equations have not been subtracted from the original equations (30) and (32) to form the more conventional internal mode set as, for example, in Bryan [1969] and Wang [1982]. Consequently there may be a slow tendency for the vertical integral of the internal mode velocities to differ from the external mode velocities. This arises because of different truncation errors in each mode. To insure against accumulated mismatch, the vertical mean of the internal velocity is replaced at every time step by the external mode velocity.

5. Finite Difference Formulation

The governing equations form a set of simultaneous partial differential equations which cannot be solved using known analytic methods. The equations require numeric computational methods using discretized equations on a grid. In anticipation of constructing the finite differencing scheme, the governing equations have been cast into their flux form. This is to insure that certain integral constraints are maintained by the differencing.

Spatial and Temporal Finite Differencing

To derive the finite difference equations, the following sum and difference operations are defined:

$$\overline{F(x,y,\sigma,t)}^{x} \equiv \frac{F(x+\frac{\Delta x}{2},y,\sigma,t) + F(x-\frac{\Delta x}{2},y,\sigma,t)}{2} \qquad (52a)$$

$$\delta_x F(x,y,\sigma,t) \equiv \frac{F(x+\frac{\Delta x}{2},y,\sigma,t) - F(x-\frac{\Delta x}{2},y,\sigma,t)}{\Delta x} \qquad (52b)$$

$$\delta_x \overline{F(x,y,\sigma,t)}^{x} \equiv \frac{F(x+\Delta x,y,\sigma,t) - F(x-\Delta x,y,\sigma,t)}{2\Delta x} \qquad (52c)$$

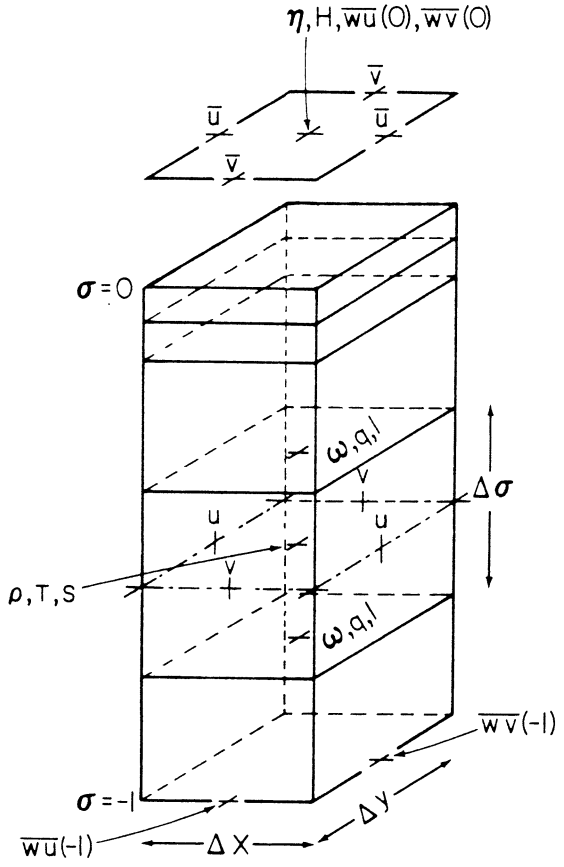

Fig. 1. The locations of the variables on the finite difference grid.

and

$$\overline{F(x,y,\sigma,t)}^{xy} \equiv \overline{\overline{F(x,y,\sigma,t)}^{x}}^{y} \equiv \overline{\overline{F(x,y,\sigma,t)}^{y}}^{x} \qquad (53)$$

the bar and delta (δ) operators form a commutative and distributive algebra. A variable $F(x,y,\sigma,t)$ can now be written as $F^{n}_{i,j,k}$. The relative positions of the variables on the staggered computational "C" grid are shown in Figure 1. The staggered arrangement uses U at points to the east and west of the point where η and H are defined and V at points to the north and south of the η and H points. This type of grid has been shown by Batteen and Han [1981] to be the most effective grid for high resolution (< 50 km grids) ocean circulation models. The Δx and Δy are the constant horizontal grid spacings and $\Delta\sigma$ is the vertical increment which varies in thickness to accommodate more resolution near the surface and bottom.

The finite difference equations governing the motion of the baroclinic (internal) modes, (30), (31), and (32) are

$$\delta_t\eta + \delta_x(\bar{D}^x U) + \delta_y(\bar{D}^y V) + \delta_\sigma(\omega) = 0 \qquad (54)$$

$$\delta_t\overline{(\bar{D}^x U)}^t + \delta_x\overline{(\bar{D}^x U\,\bar{U}^x)}^x + \delta_y\overline{(\bar{D}^y V\,\bar{U}^y)}^x - \overline{f\bar{V}^y D}^x + \delta_\sigma(\bar{W}^x\bar{U}^\sigma) + g\bar{D}^x\delta_x\eta = \delta_\sigma\left[\frac{\overline{K_M}^x}{\bar{D}^x}\delta_\sigma(U)^{n+1}\right] - \frac{g(\bar{D}^x)^2}{\rho_o}\delta_x\left[\sum_{m=1}^{k}\overline{\rho_{m-1/2}}^{\sigma}\,\overline{\Delta\sigma_{m-1/2}}^{\sigma}\right] + F_x^{n-1} \qquad (55)$$

$$\delta_t\overline{(\bar{D}^y V)}^t + \delta_x\overline{(\bar{D}^x U\,\bar{V}^x)}^y + \delta_y\overline{(\bar{D}^y V\,\bar{V}^y)}^y + \overline{f\bar{U}^x D}^y + \delta_\sigma(\bar{W}^y\bar{V}^\sigma) + g\bar{D}^y\delta_y\eta = \delta_\sigma\left[\frac{\overline{K_M}^y}{\bar{D}^y}\delta_\sigma(V)^{n+1}\right] - \frac{g(\bar{D}^y)^2}{\rho_o}\delta_y\left[\sum_{m-1}^{k}\overline{\rho_{m-1/2}}^{\sigma}\,\overline{\Delta\sigma_{m-1/2}}^{\sigma}\right] + F_y^{n=1} \qquad (56)$$

The parameter k in (55) and (56) is the number of vertical grid points over which the summation is performed and $\Delta\sigma$ is the spacing of the vertical layers. The superscripts n+1 and n-1 are used to indicate the appropriate time level. All other terms are understood to be a level n. These difference equations are similar to those proposed by Lilly [1965], Leendertse et al. [1973], Holland and Lin [1975], and Blumberg [1977]. To reduce the numerical truncation associated with density gradients in regions of large baroclinic and topographic variability, a reduced density (area mean removed) is introduced to (55) and (56).

The conservation equation for a scalar, Θ_i as in (33) and (34) is differenced as

$$\delta_t\overline{(\Theta_i D)}^t + \delta_x(\bar{\Theta}_i^x U\bar{D}^x) + \delta_y(\bar{\Theta}_i^y V\bar{D}^y) + \delta_\sigma(\bar{\Theta}_i^\sigma\omega) = \delta_\sigma\left(\frac{K_H}{D}\delta_\sigma\Theta_i\right)^{n+1} + F_{\Theta_i}^{n-1} \qquad (57)$$

The advective characteristics of this particular differencing scheme, evaluated by Kerr and Blumberg [1979], can produce a nonphysical behavior if discontinuities in the property, Θ_i, exist. The scheme introduces no artificial horizontal (or vertical) diffusion so that small scale noise generated at a discontinuity must be controlled with the explicit diffusion as is preferred. Similar differencing for the turbulence equations (35) to (36) results for the kinetic energy

$$\overline{\delta_t(q^2 D)}^t + \delta_x(\bar{U}^\sigma\overline{q^2\bar{D}^x}^x) + \delta_y(\bar{V}^\sigma\overline{q^2\bar{D}^y}^x) + \delta_\sigma\bar{\omega}^\sigma\overline{q^2}^\sigma = \delta_\sigma\left(\frac{K_q}{D}\delta_\sigma q^2\right)^{n+1} + \frac{2K_M}{D}\left[(\delta_\sigma\bar{U}^x)^2 + (\delta_\sigma\bar{V}^y)^2\right] + \frac{2g}{\rho_o}K_H\delta_\sigma\rho - \frac{2Dq^3}{B_1\ell} + F_q^{n-1} \qquad (58)$$

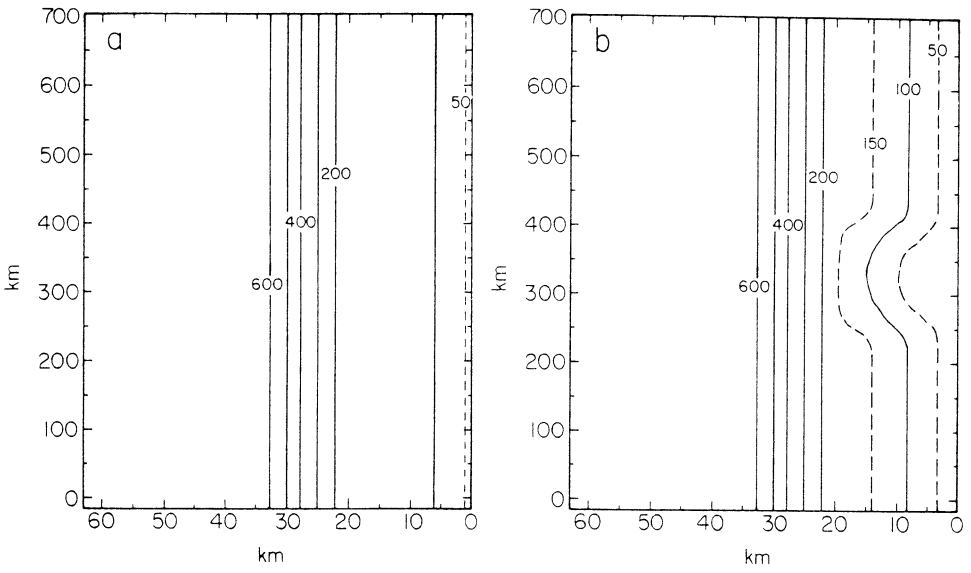

Fig. 2. The bottom topography used in the upwelling experiments. Isobaths in m. (a) The case with the northward invariant topography, and (b) the case with a topographic irregularity.

and for the quantity $q^2 \ell$,

$$\delta_t(\overline{q^2\ell D})^t + \delta_x(\bar{U}^\sigma \overline{q^2\ell}^x \bar{D}^x) + \delta_y(\bar{V}^\sigma \overline{q^2\ell}^y \bar{D}^y) + \delta_\sigma \bar{\omega}^\sigma \overline{q^2\ell}^\sigma$$
$$= \delta_\sigma\left(\frac{K_q}{D}\delta_\sigma q^2\ell\right)^{n+1} + \ell E_1 \frac{K_M}{D}\left[(\delta_\sigma \bar{U}^x)^2 (\delta_\sigma \bar{V}^y)^2\right]$$
$$+ \frac{\ell E_1 g}{\rho_o} K_H \delta_\sigma \rho - \frac{Dq^3}{B_1}\left\{1 + E_2\left[\frac{\ell}{\kappa D}\left(\frac{1}{\sigma} + \frac{1}{1+\sigma}\right)\right]^2\right\} + F_\ell^{n-1} \tag{59}$$

The implicit treatment of the vertical diffusion terms is used to accommodate the small vertical spacing required to resolve the important top and bottom boundary layers without drastically reducing the time step as would be the case with the more usual explicit schemes. The use of an implicit scheme results in a tri-diagonal matrix which is solved by a Gaussian elimination method [Richtmyer and Morton, 1967].

The external mode equations (45) through (47) are entirely explicit and are differenced for the continuity equation,

$$\delta_t \bar{\eta}^t + \delta_x(\bar{D}^x \bar{U}) + \delta_y(\bar{D}^y V) = 0 \tag{60}$$

and for the momentum equations

$$\delta_t(\overline{\bar{D}^x \bar{U}})^t + \delta_x(\overline{\bar{D}^x \bar{U}\,\bar{U}}^{x-x}) + \delta_y(\overline{\bar{D}^y V\,\bar{U}}^{x-y}) - \overline{f\bar{V}\,D}^x$$
$$+ g\bar{D}^x \delta_x \eta - \bar{F}_x^{n-1} = \Phi_x \tag{61}$$

$$\delta_t(\overline{\bar{D}^y \bar{V}})^t + \delta_x(\overline{\bar{D}^x \bar{U}\,\bar{V}}^{y-x}) + \delta_y(\overline{\bar{D}^y V\,\bar{V}}^{y-y}) + \overline{f\bar{U}\,D}^y$$
$$+ g\bar{D}^y \delta_y \eta - \bar{F}_y^{n-1} = \Phi_y \tag{62}$$

The structure functions, Φ_x and Φ_y, are composed of quantities in (46) and (47) provided by the internal mode and are computed by vertical integration of the corresponding terms in the internal mode equation using the rectangular rule. The finite difference version of the horizontal viscosity and diffusion is not presented here as these terms are exceedingly cumbersome but straightforward.

The finite difference equations presented above can be demonstrated to be of second order accuracy in space and time and to conserve energy, temperature, salinity, mass, and momentum. Finally, the model's computer code has been deliberately designed to be economical on modern array processing computers.

Stability Constraints

The leap-frog differencing used for the time stepping introduces a tendency for the solution at even and odd time steps to split. This time splitting is removed by a weak filter [Asselin, 1972] where the solution is smoothed at each time step according to

$$F_s^n = F^n + \frac{\alpha}{2}(F^{n+1} - 2F^n + F_s^{n-1}) \tag{63}$$

where $\alpha = 0.05$ and F_s is a smoothed solution.

TABLE 1. The Vertical σ Coordinate Distribution

Level	σ	σ'	Δσ
1	0.00000		
		-0.01042	0.02083
2	-0.02083		
		-0.02946	0.02083
3	-0.04167		
		-0.05893	0.04167
4	0.08333		
		-0.11785	0.08333
5	-0.16667		
		-0.20833	0.08333
6	-0.25000		
		0.29167	0.08333
7	-0.33333		
		-0.37500	0.08333
8	-0.41667		
		-0.45833	0.08333
9	-0.50000		
		-0.54167	0.08333
10	-0.58333		
		-0.62500	0.08333
11	-0.66667		
		-0.70833	0.08333
12	-0.75000		
		-0.79167	0.08333
13	-0.83333		
		-0.88215	0.08333
14	-0.91667		
		-0.94107	0.04167
15	-0.95833		
		-0.97917	0.04167
16	-1.00000		

The quantity σ refers to the depths at which the turbulence quantities and the vertical velocity are located, while σ' corresponds to the depth at which horizontal velocity, temperature, salinity, and denisty are defined. The Δσ is the grid spacing. The relative position of the variables is shown in Figure 1.

This technique introduces less damping than either the Euler-backward or forward stepping techniques.

The Courant-Friedrichs-Levy (CFL) computational stability condition on the vertically integrated, external mode, transport equations limits the time step as shown by Blumberg and Mellor [1981a] according to

$$\Delta t \leq \frac{1}{C_t}\left(\frac{1}{\Delta x^2}+\frac{1}{\Delta y^2}\right)^{-1/2} \qquad (64a)$$

where

$$C_t = 2(gH)^{1/2} + \bar{U}_{max} \qquad (64b)$$

$\bar{U}_{max}$ is the maximum average velocity expected. There are other restrictions but in practice the CFL limit is the most stringent. The model time step is usually 90% of this limit. The internal mode has a much less stringent time step since the fast moving external mode effects have been removed. The time step criteria is analogous to the one for the external mode given by (64a) and is

$$\Delta T \leq \frac{1}{C_t}\left(\frac{1}{\Delta x^2}+\frac{1}{\Delta y^2}\right)^{-1/2} \qquad (65)$$

where $C_T = 2C + U_{max}$, with C being the maximum internal gravity wave speed commonly of order 2m/s and U_{max} is the maximum advective speed. For typical coastal ocean conditions the ratio of the time steps, $\Delta T/\Delta t$, is often a factor of 80-100.

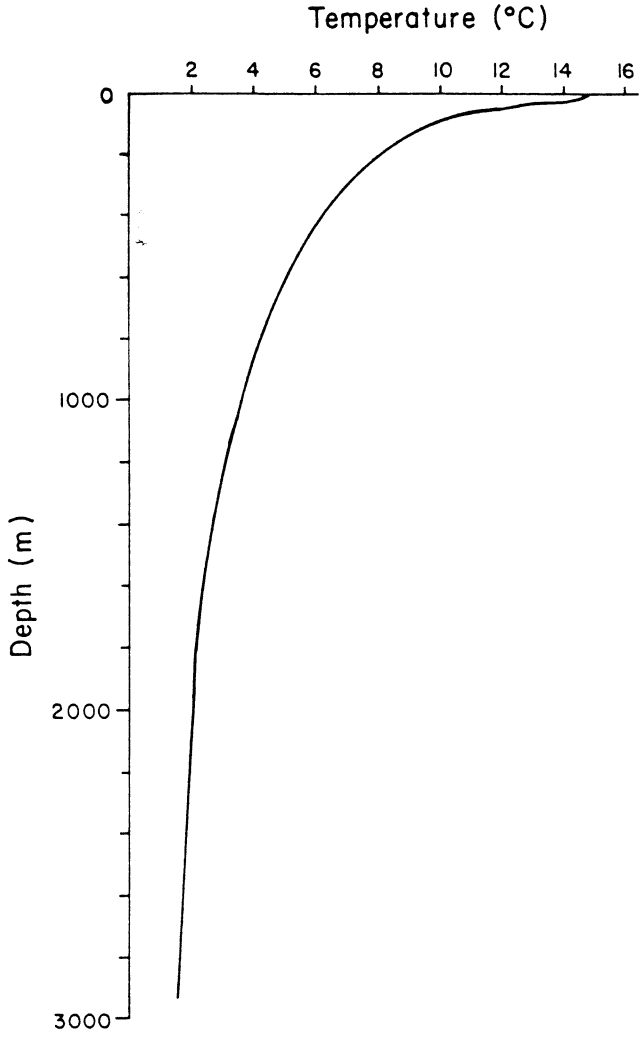

Fig. 3. The initial temperature distribution used in the prognostic model experiments. The distribution is typical of that observed off the coast of California.

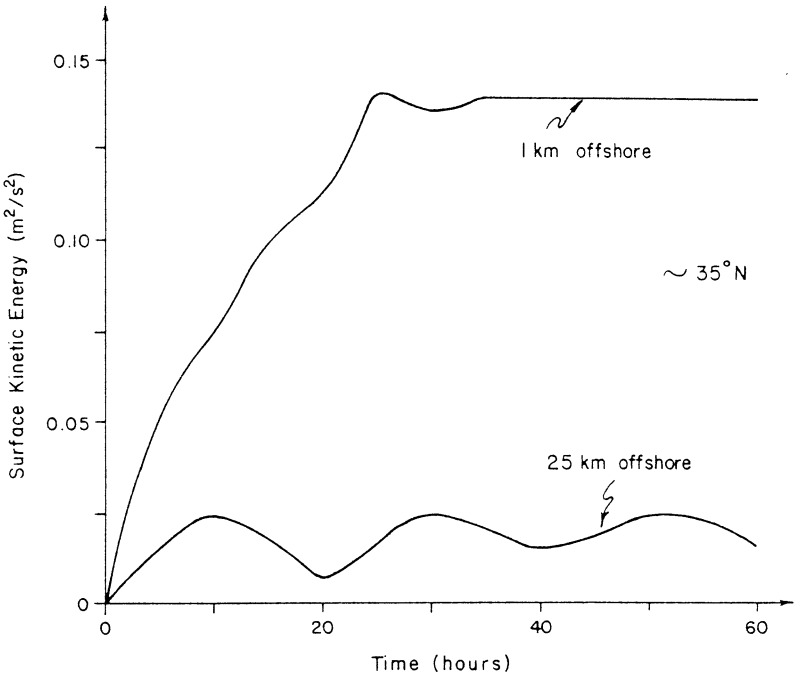

Fig. 4. Time history of the surface kinetic energy at two positions offshore; results from the prognostic model upwelling experiment.

Diffusion is important in the internal mode but does not affect the overall choice of time step, unless the grid Reynolds number is of order 1, in which case

$$\Delta T \leq \frac{1}{4A_H}\left(\frac{1}{\Delta x^2}+\frac{1}{\Delta y^2}\right)^{-1} \qquad (66)$$

must be used.

A rotational condition is

$$\Delta t < \frac{1}{f} = \frac{1}{2\Omega \sin\theta} \qquad (67)$$

where Ω is the angular velocity of the earth and θ is the latitude. However, even for high latitudes (67) is not a limiting factor.

6. Application: Upwelling Coastal Trapped Waves

To illustrate an application of the circulation model, a calculation not previously presented in the literature will be described. For additional applications the reader is referred to the references cited in the introduction. For the purposes of this paper, it is appropriate to investigate in a simpler context some of the characteristics of upwelling and eastern boundary currents. This approach helps to establish model credibility and also provides a framework for extending the model to include geographical settings where the circulation can be indeed complex.

Consider the response of a stratified ocean adjacent to a meridional boundary to the onset of equatorward (upwelling favorable) winds. A rectangular ocean basin 65 km wide and 700 km in north-south extent centered about latitude 36°N is used. The basin has a continental shelf-slope with characteristics typical of northern California as shown in Figure 2a. Alongshore variation in topography is not considered initially. The east-west grid spacing is 2 km and the north-south spacing is 30 km. Because this is a limited domain in spatial extent, that is, an enclosed basin, only short duration experiments can be considered. Otherwise disturbances generated at the boundaries become an important although artificial contribution to the response.

The model consists of 16 vertical levels with irregular vertical spacing in σ space as shown in Table 1. The initial temperature distribution is horizontally homogeneous with a vertical structure similar to that observed off California (~35°N, 125°W). A strong thermocline is present at a depth of ~150 m as shown in Figure 3. The salinity distribution, on the other hand, is set everywhere equal to 34 per mil and used as a check on the conservation properties of the finite difference technique. The horizontal mixing coefficients are both chosen as 50 m^2/s. The external and internal mode time steps are limited to 10 s and 10 min respectively. A meridional, equatorward, 2 $dyne/cm^2$ wind stress is impulsively imposed at the surface in a 240-km-wide zonal band about 200 km from the southern edge of the domain. There is no wind stress curl or heat flux

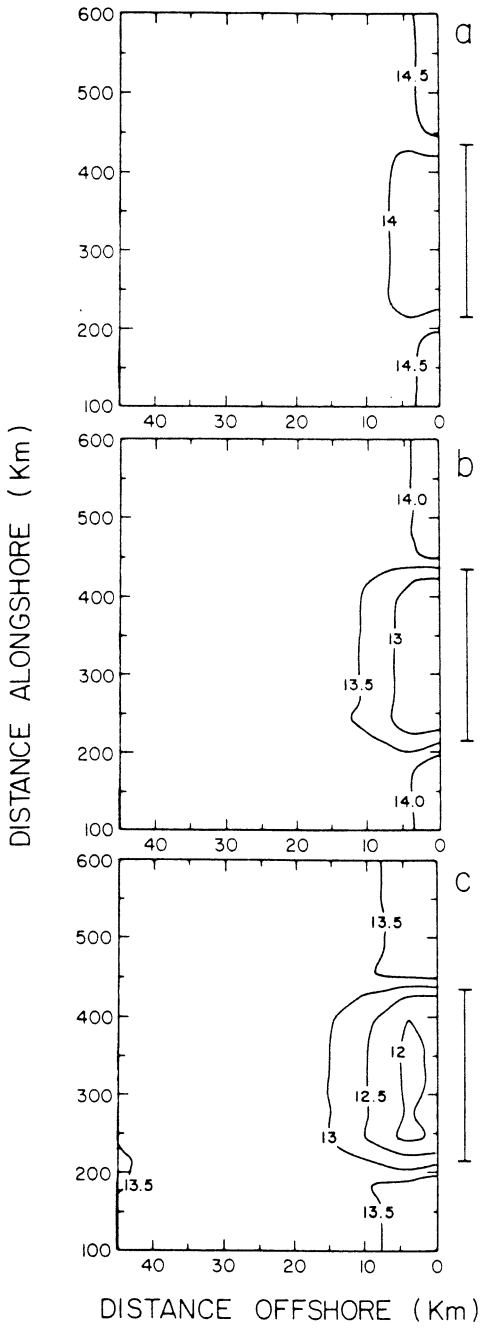

Fig. 5. The surface temperature (°C) distributions from the upwelling experiment after (a) 20 hours, (b) 40 hours, and (c) 60 hours. The forcing region is marked on the right side of each figure.

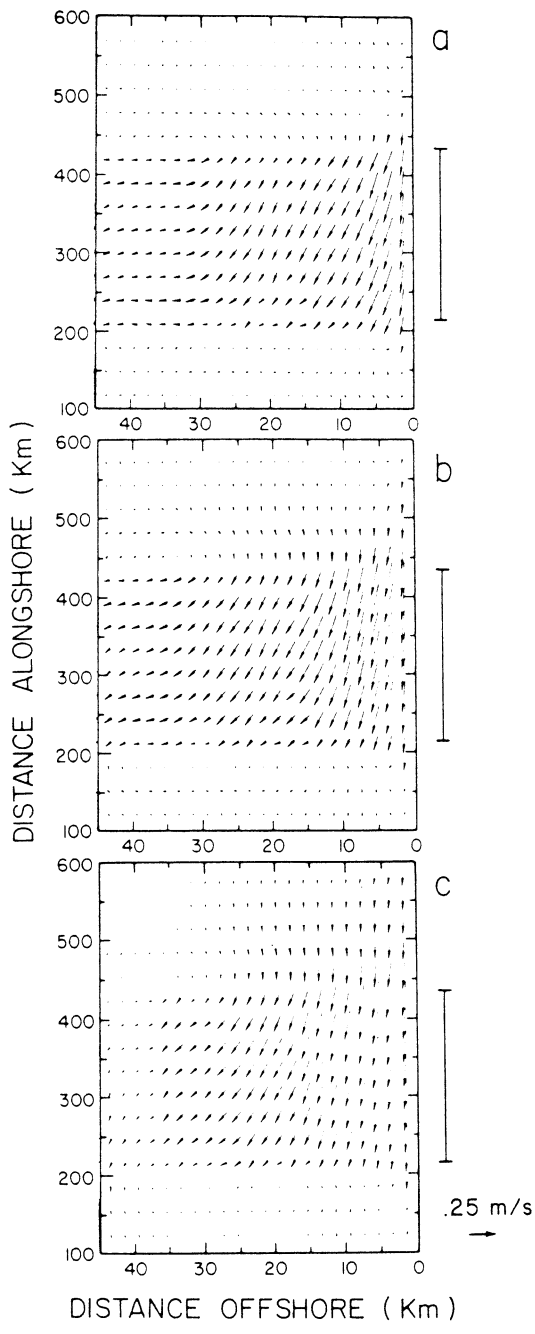

Fig. 6. The near surface circulation patterns from the upwelling experiment after (a) 20 hours, (b) 40 hours, and (c) 60 hours. The forcing region is marked on the right side of each figure.

imposed. The radius of deformation for the initial stratification is ~10 km and is smaller than the width of the shelf-slope, the ratio is ~0.5.

The time history of surface kinetic energy for the 2-1/2-day simulation at locations 1 and 25 km offshore is shown in Figure 4. Inertial motions are clearly evident with the proper 20-hour period (~ 35°N). The shelf water response to the wind is illustrated in Figures 5-9. Sequential patterns at 20-hour intervals spanning 60 hours of the horizontal distributions of surface temperature, surface velocity, and 100-m-depth velocity are depicted. Also included are patterns

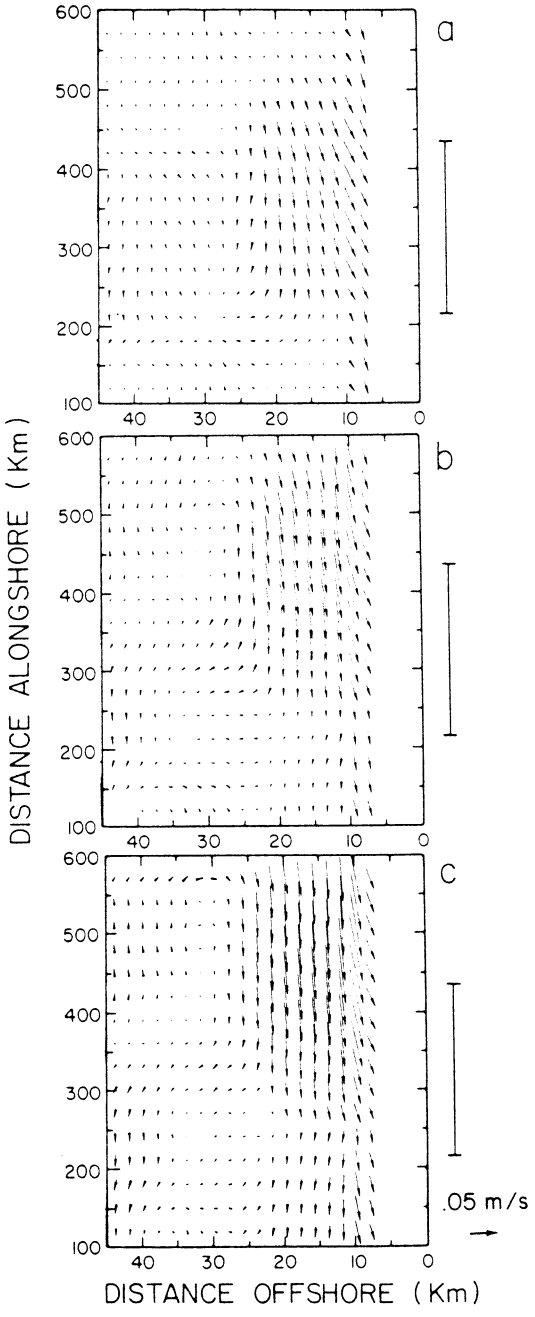

Fig. 7. The 100-m-depth circulation patterns from the upwelling experiment after (a) 20 hours, (b) 40 hours, and (c) 60 hours. The forcing region is marked on the right side of each figure.

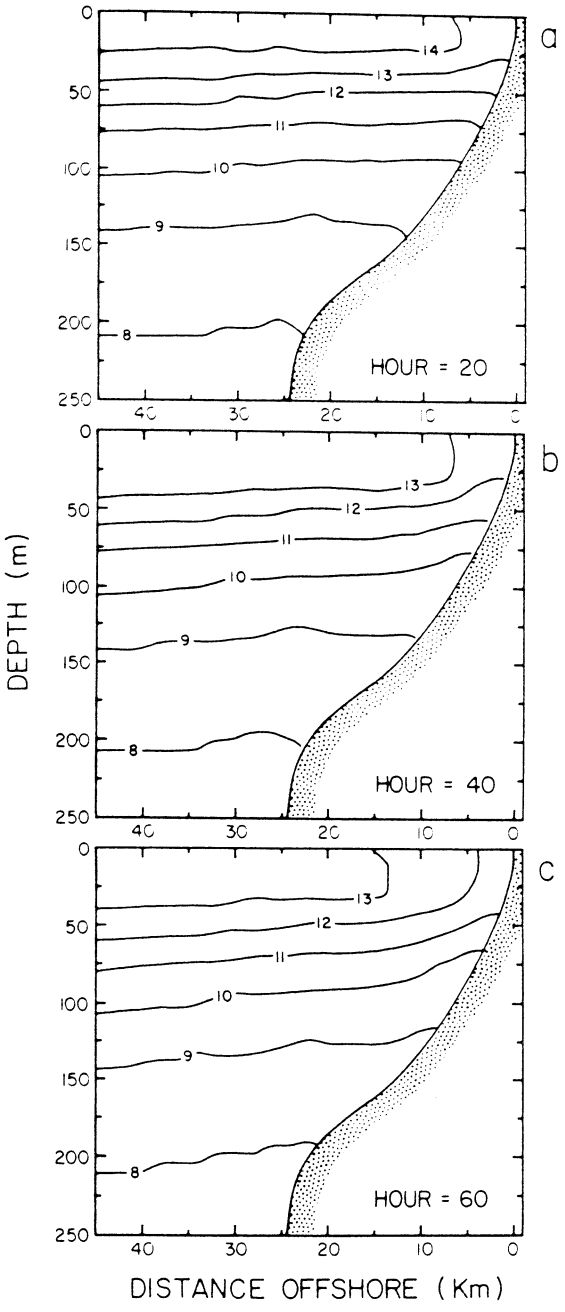

Fig. 8. Sequential patterns of temperature along a vertical section near the northern edge of the wind forcing zone (CI = 1°C).

of the temperature and alongshore velocity from a vertical section near the northern edge of the forcing zone. An intense downwelling response exists on the western boundary. To focus upon the upwelling regime, only the eastern boundary region is shown in these figures.

The initial response to the onset of the winds is the classical Ekman surface offshore flow and the compensating onshore flow at depth. Intense coastal upwelling is found within the forcing zone (see Figures 5 and 8). As time progresses the onshore circulation decreases in strength and the flow becomes markedly three-dimensional. The equatorward jet is confined to the coastal region. As proposed by Philander and Yoon [1982],

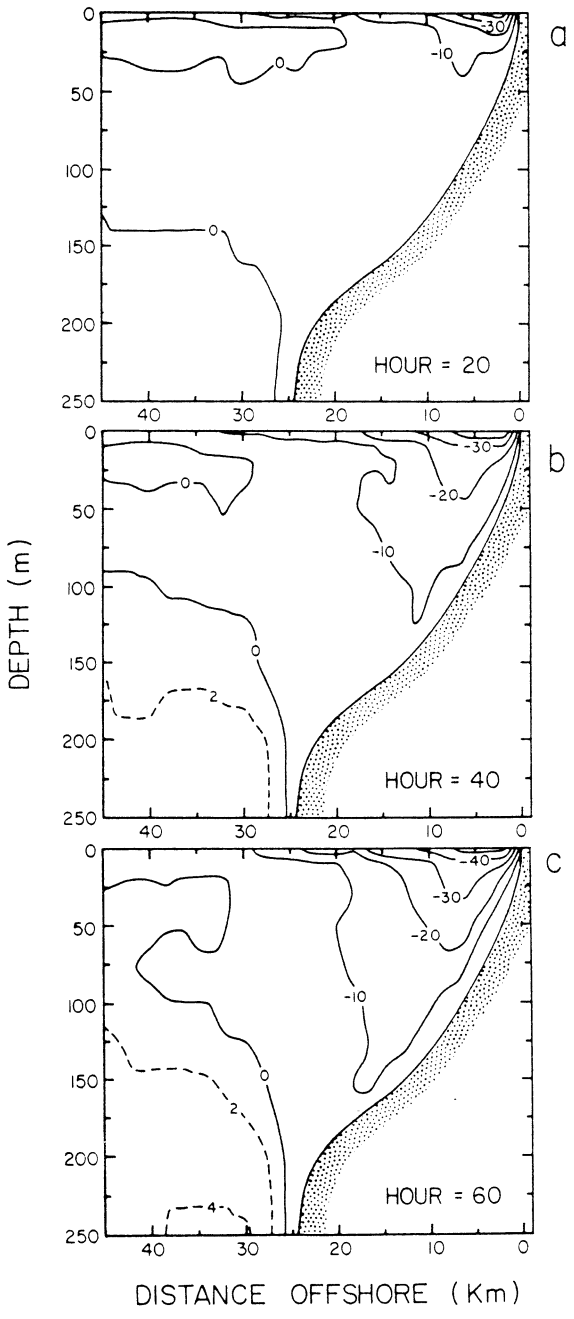

Fig. 9. Sequential patterns of alongshore velocity along a vertical section near the northern edge of the wind forcing zone (CI = 10 cm/s).

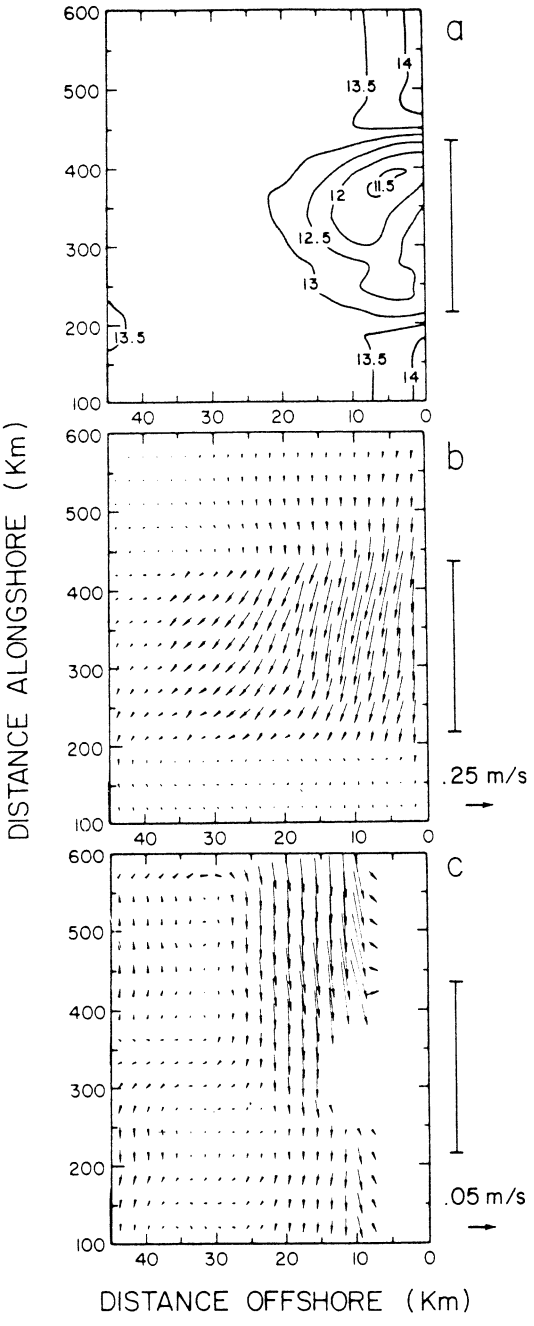

Fig. 10. The surface temperature (°C) distribution (a) and the near surface (b) and 100-m-depth (c) circulation patterns after 60 hours from the upwelling experiment with the topographic irregularity. The forcing region is marked on the right side of each figure.

Suginohara [1982], and Wang [1982] and corroborated here, the limited area wind leads to the generation of coastal trapped waves which propagate northward. The first mode waves travel at ~250 km/day. A poleward undercurrent (see Figure 9) develops below the thermocline over the slope region at ~250 m depth when the second mode coastal trapped wave arrives, travelling at ~80 km/day, from the southern edge of the forcing zone. The poleward current is apparently produced by an alongshore pressure gradient which propagates into the forcing region. It should be re-

marked that the inertial effects are responsible for offshore surface currents not always being aligned with the wind.

In the next numerical experiment the effect of alongshore variations of bottom topography is investigated. A schematic view of the topography is illustrated in Figure 2b. The length scale of the topographic irregularity is much larger than the Rossby deformation radius. Figure 10 shows the surface temperature and circulation and the 100-m-depth circulation 60 hours after the sudden onset of a limited area, upwelling favorable, 2 dyne/cm^2 wind stress. The most striking feature in Figure 10 is the enhanced upwelling which occurs over the northern edge of the topographic feature which was not present in Figure 5c. There is also some enhancement at the southern edge but to a lesser extent. The rate of upwelling is also greater when the topographic feature is included. The results obtained here are corroborated by those of Kishi and Suginohara [1975]. In both of the present numerical experiments, salinity was conserved to within machine accuracy.

While there is always some uncertainty as to the ultimate cost of a computation, the 2-1/2-day experiment with a 32 x 24, 16-level model with 144 time steps per day requires 1.0 min/day on a Cray-1S computer. The numerical experiments described here indicate that the circulation model is operational and is capable of representing the physical processes responsible for the three-dimensional behavior of the coastal ocean. By virtue of providing reliable dynamic and thermodynamic properties, it is believed that this circulation model will be useful for forecasting the behavior of coastal ocean regions.

7. Conclusions

A three-dimensional, coastal ocean circulation model has been described in detail. The model, originally designed for carrying out coastal ocean predictions, has been extended to include estuaries as well as whole basins, like the Gulf of Mexico, and to operate in both prognostic and diagnostic modes.

The vertical coordinate representation, the mode splitting technique and the open boundary conditions have been emphasized. An apparently unique feature of the circulation model is its turbulence closure submodel which should provide accurate surface and bottom mixed layer dynamics. An enhancement, now in progress, is to replace the present rectangular horizontal grid with an orthogonal, curvilinear horizontal grid to improve coastline representations.

To illustrate the utility of the circulation model, it was applied to a coastal upwelling situation. It appears from an examination of the simulation that the model yields results that share many features in common with our understanding of upwelling and coastal trapped waves. However, more qualitative comparisons between model and data/theory are necessary. It is only through these comparisons that one can understand and assess the model's predictive capabilities and limitations.

Acknowledgments. The development of the model was supported over the years by a variety of sources. In particular the authors wish to acknowledge the support provided by the Office of Sea Grant/NOAA/U.S. Department of Commerce, the New Jersey Marine Sciences Consortium, the Division of Solar Technology/U.S. Department of Energy under contract number DE-AC02-78ET20612, and the Bureau of Land Management and the Minerals Management Service of the U.S. Department of the Interior under contracts AA551-CT9-32 and AA851-CT1-67. This article was prepared with support from the Dynalysis Fund for Independent Research and Development. The authors are indebted to H. James Herring for his efforts in providing an environment conducive to research.

References

Asselin, R., Frequency filters for time integrations, Mon. Weather Rev., 100, 487-490, 1972.

Batteen, M. L., and Y.-J. Han, On the computational noise of finite-difference schemes used in ocean models, Tellus, 33, 387-396, 1981.

Beardsley, R. C., and W. C. Boicourt, On estuarine and continental-shelf circulation in the Middle Atlantic Bight, in Evolution of Physical Oceanography, edited by B. A. Warren and C. Wunsch, pg. 198-234, MIT Press, Cambridge, Mass., 1981.

Blumberg, A. F., Numerical tidal model of Chesapeake Bay, J. Hydraul. Div., 103, 1-10, 1977.

Blumberg, A. F., and L. H. Kantha, Open boundary condition for circulation models, J. Hydraul. Eng., 111, 237-255, 1985.

Blumberg, A. F., and G. L. Mellor, A whole basin model of the Gulf of Mexico. Proc. 6th Ann. Conf. on OTEC, Department of Energy, Washington, D.C., 13.15-1 to 13.15-10, 1979a.

Blumberg, A. F., and G. L. Mellor, The potential impact of three-dimensional circulation modelling on oil spill forecasting, in The Physical Behavior of Oil in the Marine Environment, Princeton University, Department of Civil Engineering, 6.1-6.18, 1979b.

Blumberg, A. F., and G. L. Mellor, A coastal ocean numerical model, in Mathematical Modelling of Estuarine Physics, Proc. Int. Symp., Hamburg, August 24-26, 1978. edited by J. Sundermann and K.-P. Holz, 203-214, Springer-Verlag, Berlin, 1980.

Blumberg, A. F., and G. L. Mellor, A numerical calculation of the circulation in the Gulf of Mexico, Dynalysis of Princeton, Report No. 66, 153 pp., 1981a.

Blumberg, A. F., and G. L. Mellor, Some results from a Gulf of Mexico circulation model, in Proc. 8th Ocean Energy Conf., Department of Energy, Washington, D.C. pp. 483-493, 1981b.

Blumberg, A. F., and G. L. Mellor, Diagnostic and prognostic numerical circulation studies of the

South Atlantic Bight, J. Geophys. Res, 88, 4579-4592, 1983.

Bryan, K., A numerical method for the study of the circulation of the world ocean, J. Comput. Phys., 4, No. 3, 347-376, 1969.

Fofonoff, N. P., Physical properties of sea-water, in The Sea, Vol. 1, edited by N. M. Hill, pp. 3-30, Interscience, New York, 1962.

Hanjalic, K., and B. E. Launder, Fully developed asymmetric flow in a plane channel, J. Fluid Mech., 52, 689, 1972.

Holland, W. R., and L. B. Lin, On the generation of mesoscale eddies and their contribution to the oceanic general circulation, I. A preliminary numerical experiment, J. Phys. Oceanogr., 5, 642-657, 1975.

Kantha, L. H., G. L. Mellor, and A. F. Blumberg, A diagnostic calculation of the general circulation in the South Atlantic Bight, J. Phys. Oceanogr., 12, 805-819, 1982.

Kerr, C. L., and A. F. Blumberg, An analysis of a local second-moment conserving quasi-Lagrangian scheme for solving the advection equation, J. Comput. Phys., 32, 1-9, 1979.

Kishi, M. J., and N. Suginohara, Effects of longshore variation of coastline geometry and bottom topography on coastal upwelling in a two-layer model, J. Oceanogr.Soc. Japan, 31, 48-50, 1975.

Leendertse, J. J., R. C. Alexander, and S.-K. Liu, A three-dimensional model for estuaries and coastal seas, Volume I, Principles of Computation, The Rand Corp., Santa Monica, Calif., R-1417-OWRR, 1973.

Lilly, D. K., On the computational stability of numerical solutions of time-dependent nonlinear geophysical fluid dynamics problems, Mon. Weather Rev., 93, 11-26, 1965.

Madala, R. V., and S. A. Piacsek, A semi-implicit numerical model for baroclinic oceans, J. Comput. Phys., 23, 167-178, 1977.

Mellor, G. L., Analytic prediction of the properties of stratified planetary surface layers, J. Atmos. Sci., 30, 1061-1069, 1973.

Mellor, G. L., and A. F. Blumberg, Modelling vertical and horizontal diffusivities and the sigma coordinate system, Mon. Weather Rev., 113, 1379-1383, 1985.

Mellor, G. L., and H. J. Herring, A survey of the mean turbulent field closure models, AIAA J., 11, 590-599, 1973.

Mellor, G. L., and T. Yamada, A hierarchy of turbulence closure models for planetary boundary layers, J. Atmos. Sci., 31, 1791-1896, 1974.

Mellor, G. L., and T. Yamada, Development of a turbulence closure model for geophysical fluid problems, Rev. Geophys. Space Phys., 20, No. 4, 851-875, 1982.

Philander, S.G.H., and J.-H. Yoon, Eastern boundary currents and coastal upwelling, J. Phys. Oceanogr., 12, No. 8, 862-879, 1982.

Phillips, N. A., A coordinate system having some special advantages for numerical forecasting, J. Meteorol., 14, 184-185, 1957.

Richtmyer, R. D., and K. W. Morton, Difference Methods for Initial-Value Problems, Second Edition, Interscience, New York, 1967.

Simons, T. J., Verification of numerical models of Lake Ontario, Part I. Circulation in spring and early summer, J. Phys. Oceanogr., 4, 507-523, 1974.

Smagorinsky, J., General circulation experiments with the primitive equations, I. The basic experiment, Mon. Weather Rev., 91, 99-164, 1963.

Suginohara, N., Coastal upwelling: Onshore-offshore circulation, equatorward coastal jet and poleward undercurrent over a continental shelf-slope, J. Phys. Oceanogr., 12, No. 3, 272-284, 1982.

Wang, D.-P., Development of a three-dimensional, limited-area (island) shelf circulation model, J. Phys. Oceanogr., 12, 605-617, 1982.

Weatherly, G., and P. J. Martin, On the structure and dynamics of the ocean bottom boundary layer, J. Phys. Oceanogr., 8, 557-570, 1978.